Photo-degradation of Acid-red 3B dye catalyzed by TiO$_2$ nanotubes

JIANG Fang, ZHENG Shou-rong, ZHENG Zheng*, XU Zhao-yi, WANG Yan-jin

(State Key Laboratory of Pollution Control and Resource Reuse, School of the Environment, Nanjing University, Nanjing 210093, China. E-mail: zzheng@nju.edu.cn)

Abstract: TiO$_2$ nanotube precursor was synthesized by the hydrothermal reaction of TiO$_2$ powders with NaOH solution and the properties of the nanotube materials were tuned using different post-treatments. Transmission electron microscopic (TEM) observation revealed that the nanotube could be obtained by either a direct rinse with acid solution or rinse with distilled water followed by acid solution. The results of X-ray diffraction (XRD) and inductively coupled plasma (ICP) analysis indicated that the nanotube material was composed of H$_2$Ti$_2$O$_5$·H$_2$O. In addition, the photocatalytic activities of the resulting catalysts were found to be strongly dependent on the post-treatment. The results of the photocatalytic reaction showed that the degradation of Acid-red 3B dye fitted pseudo-zero-order kinetics and TiO$_2$ nanotube prepared under direct rinse with acid solution exhibited a higher catalytic efficiency compared to other catalysts.

Keywords: TiO$_2$ nanotube; Acid-red 3B; photocatalysis; hydrothermal reaction

Introduction

As one kind of novel functional material, TiO$_2$ nanotube has been found potential applications in solar cell (Barbe et al., 1997), semiconductor device (Vinodgopal et al., 1993) and catalyst supports (Idakiev et al., 2005) etc. Since Kasuga et al. (1998) reported the preparation of TiO$_2$ nanotube using a hydrothermal method in 1998, special attention has been recently paid to the exploration of the preparation methods, formation mechanism and composition of TiO$_2$ nanotube (Bavykin et al., 2004; Chen et al., 2002; Yang et al., 2003; Wang et al., 2004; Yoshida et al., 2005). However, the general agreement has not been reached regarding the formation mechanism and structural composition of this novel material. Kasuga et al. (1998, 1999) concluded that TiO$_2$ nanotube consisted of titanium oxide (anatase phase). In contrast, Du et al. (2001) suggested that TiO$_2$ nanotube mainly contained TiO$_x$ rather than TiO$_2$. Some research groups believed that TiO$_2$ nanotube was built in a layered titanate structure, possibly H$_2$Ti$_3$O$_7$ (Chen et al., 2002). While Ma et al. (2003) suggested that TiO$_2$ nanotube was constructed from lepidocrocite H$_x$Ti$_{2-x/4}\square_{x/4}$O$_4$ (x: 0.7, $\square$: vacancy) sheets rather than trititanate. Recently, Yang et al. (2003) and Zhang et al. (2004) found that the composition of such a nanotube material had a chemical component of Na$_2$Ti$_2$O$_4$(OH)$_2$ or H$_2$Ti$_2$O$_4$(OH)$_2$.

In this study, we investigated the applications of TiO$_2$ nanotube as the photocatalyst in the abatement of environmental pollutants. Note that the production of dye has led to extensive pollution in waters in China. Furthermore, azo dyestuff is the most used and produced dye. As one of the representative azo dyestuff, Acid-red 3B, whose structure is shown in Fig.1, was also extensively produced and used. The treatment of the wastewater containing azo dyestuff using adsorption (Saha et al., 2005), ozonation oxidation (Koch et al., 2002), ultrasonic oxidation (Ge and Qu, 2003) and photocatalytic decomposition (Zheng et al., 1997, 2005) was attempted to remove the dye from aqueous environment. Among these treatment methods, photocatalytic decomposition was found to be one of the most effective approaches due to its high treatment efficiency and the complete mineralization of the dye molecule. In this study, therefore, Acid-red 3B was selected as the typical organic pollutant and used to evaluate the photo-catalytic efficiency of nanotube.
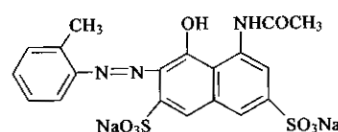
1 Experimental

Fig.1   Structure of Acid-red 3B

1.1 Preparation of catalysts

TiO$_2$ nanotube was prepared using the hydrothermal method followed by different post-treatments. Typically, 2 g TiO$_2$ powder (Shanghai Sanpu Ltd. Corp., Shanghai, China) was added into 40 ml of 10 mol/L NaOH aqueous solution and the suspension system was stirred for 2 h at room temperature. Then, the mixture was transferred to a teflon-lined stainless autoclave and heated at 150℃ for 72 h. After the autoclave cooled down to room temperature, the solution was decanted and the solid was broken into small particles followed by drying at 80℃. The resulting TiO$_2$ nanotube precursor denoted as TN-P. As for the post-treatment, one portion of TN-P was repeatedly rinsed with distilled water until the effluent was neutral. The solid was dried at 60℃ and denoted as TN-W. Portion of TN-W further

---

reacted with 0.5 mol/L HCl solution with the final pH value adjusted to 2.5. After stirring for 2 h, the solid was separated by filtration and washed with distilled water until the effluent was neutral. The resulting material was dried at 60℃ and denoted as TN-WA. Portion of TN-P was also treated directly with HCl solution at pH 2.5 adjusted using 0.5 mol/L HCl solution. Due to a large amount of residual NaOH in TN-P, a markedly larger amount of HCl solution was used to adjust solution pH to 2.5 compared to the preparation of TN-WA. The mixture was stirred for 2h, followed by centrifugation and repeated washing with distilled water to remove the extra HCl. The material was finally dried at 60℃ and denoted as TN-A.

1.2 Characterization

X-ray diffraction (XRD) patterns of the nanotube samples were collected in a Rigaku D/max-RA powder diffraction-meter using Cu Kα radiation. Transmission electron microscopic (TEM) observation was conducted with a JEM-200CX electron microscope. The BET surface areas of these materials were determined by N_2 adsorption on a Micrometrics ASAP 2020 apparatus at 77.3 K. Inductively coupled plasma (ICP) data was gathered from J-A1100 type of Jarrell-ASH.

1.3 Adsorption isotherms of Acid–red 3B

Adsorption isotherms of Acid-red 3B over the catalysts were obtained using the static adsorption method. Typically, 0.1 g of catalyst was suspended in 20 ml Acid-red 3B solution in 100 ml conical flasks with initial concentrations ranging from 10 to 500 mg/L. The conical flasks were shaken in the dark at 20℃ for 12 h. The catalyst powders were removed by filtration and the residual concentration of Acid-red 3B in the solution was determined spectro-photometrically.

The adsorption amount of Acid-red 3B dye on the sample was calculated according to Equation (1):

$$Q_c = (C_0 - C_c)V/M \tag{1}$$

where Q_c is the equilibrium adsorption amount; C_0 is the initial concentration of the dye; C_c is the equilibrium concentration of the dye; V is the volume of dye solution and M is the mass of the catalyst sample.

Under our experimental conditions, the difference of the dye concentration before and after adsorption onto TN-W catalyst was almost undetec-table due to its especially small adsorption capacities. Therefore, the adsorption isotherms of the dye on TN-A and TN-WA were measured.

1.4 Photocatalytic activity

The catalytic activities of three catalysts, TN-W, TN-WA and TN-A, for Acid-red 3B photo-degradation were investigated. The photo-degradation

was carried out in a NDC reactor equipped with a 500 ml thermostatted cylindrical Pyrex vessel irradiated directly by a high pressure mercury lamp (500 W). In a typical run, 0.5 g of the catalyst was suspended in 500 ml of 200 mg/L Acid-red 3B solution in the dark for 60 min to reach the adsorption equilibrium prior to the photo-degradation experiment. During the photo-reaction, samples were collected at selected time intervals. The catalyst powders were removed by filtration and the residual concentration of Acid-red 3B was determined spectro-photometrically.

2 Results and discussion

2.1 Catalyst characterization

The XRD patterns of the obtained three catalysts after different post-treatment are depicted in Fig.2. It was found that TN-A and TN-WA gave the similar XRD patterns and the diffraction peaks corresponding to the (200), (110), (310), (020) planes indicated that TN-A and TN-WA were composed of a layered titanate indexed to $H_2Ti_2O_5 \cdot H_2O$(JCPDS: 47-0124). This is in good agreement with the conclusion of Zhang *et al.* (2004). It is noteworthy that the diffraction peak intensity of (200) plane of TN-A was stronger than that of TN-WA, suggesting a higher structural regularity of TN-A or/and higher content of layered titanate in TN-A compared to that in TN-WA. In contrast, only broad XRD diffraction peaks were observed for TN-W. This clearly indicated that the layered titanate with low regularity or amorphous TiO_2-based species was present in TN-W.
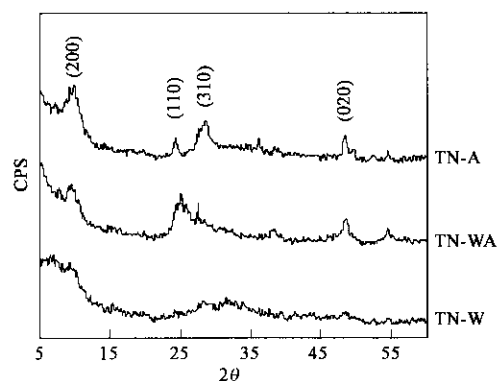

Fig.2 XRD patterns of TN-A, TN-WA and TN-W catalysts

TEM analysis was carried out to observe the microstructure of these materials and the TEM images of TN-P, TN-W, TN-WA and TN-A were compiled in Fig.3. In Fig.3a, aggregated particles with diameter ranging from 40 to 80 nm was observed, indicating that under our preparation conditions TN-P did not contain TiO_2 nanotubes. After water washing, TN-W was mainly composed of particles and nanosheets, suggesting that water washing led to partial exfoliation of TN-P into two-dimensional nanosheets and TiO_2

nanotube could not be obtained by post-treatment only using water washing. However, the presence of acid solution led to the generation of TiO$_2$ nanotube. For TN-WA, nanotubes, nanosheets and small amount of particles were observed. Note that the resulting nanotubes were not regular and it is very difficult to accurately identify the diameters of the nanotube. While for TN-A, TEM analysis indicated that TiO$_2$ particles were completely converted into nanotubes without the presence of particles and nanosheets. In addition, the nanotube exhibited a high regularity with the diameter of approximately 8—10 nm.
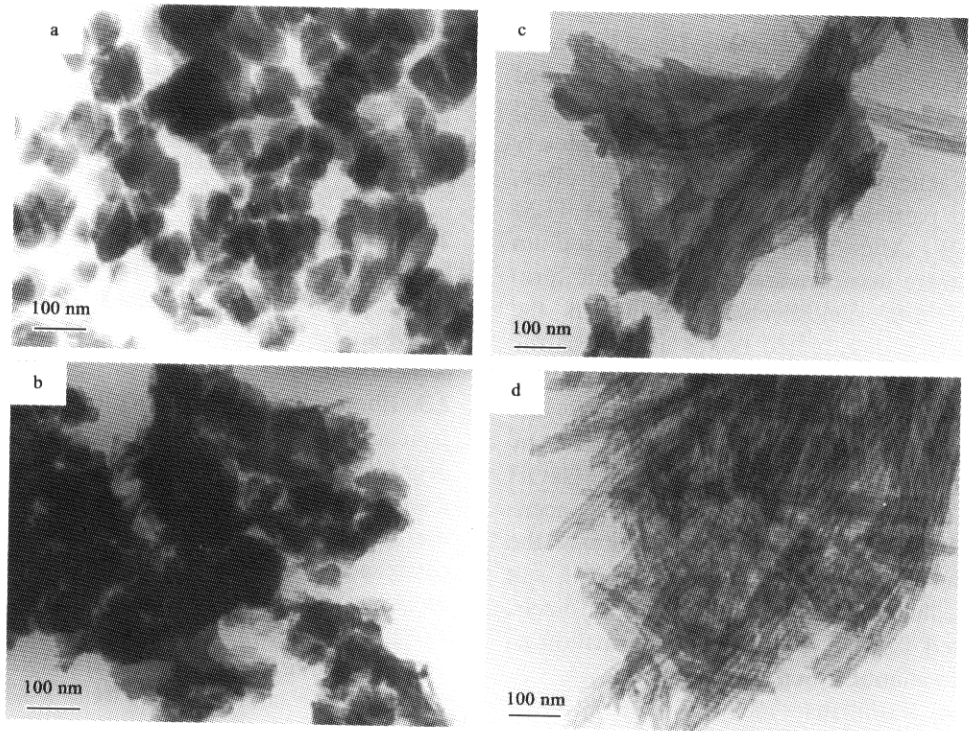

Fig.3 TEM images of catalysts
a. TN-P; b. TN-W; c. TN-WA; d. TN-A

In order to elucidate the structural difference resulted from different post-treatment, ICP analysis was conducted to differentiate the composition of the materials. The contents of Ti and Na in the three catalysts were summarized in Table 1. For TN-A and TN-WA, the contents of Na were found to be minor. In addition, the contents of titanium in the two materials were identical. Note that the content of titanium in H$_2$Ti$_2$O$_5$·H$_2$O is 48.9%, which is approximately identical to those in TN-A and TN-WA. This further proved that TN-A and TN-WA were composed of layered titanate. In TN-W, however, a marked amount of sodium was detected and the molar ratio of Ti to Na was found to be 2.4.

The BET surface areas and pore volume of the catalysts are listed in Table 1. For the TN-W, the BET surface area was 26.9 m^2/g. After further acid washing, the surface area increased markedly and almost identical BET surface area of TN-A to that of TN-WA was observed. The increased surface areas of TN-A and TN-WA could be contributed to the fact that the precursor was first exfoliated into nanosheets under acidic condition, and both the highly dispersed nanosheets and the nanotubes from the rollup of the nanosheets were accounted for the markedly elevated BET surface area (Wei et al., 2005). In addition, the pore volumes of TN-W, TN-WA and TN-A were found to be 0.11, 0.17 and 0.27 cm^3/g, respectively, which indicating that the formation of nanotube in TN-A markedly increased its pore volume. In parallel, TEM observation showed the absence of nanotubes in TN-W, which suggested that the pores in TN-W were mainly resulted form the particle aggregation. The lower pore volume of TN-WA compared to TN-A was attributed to the incomplete formation of nanotube. It is noteworthy that the average pore size of TN-A was 7.68 nm, which was in good agreement with the TEM observation.

Typically, titanate sheet rollup mechanism was used to explain the formation of TiO$_2$ nanotube. The

Table 1 Properties of the three catalysts

Catalyst	ICP, %		BET, m^2/g	Pore size, $\times 10^{-1}$ nm	Pore volume, cm^3/g
	Ti	Na			
TN-W	42.2	8.43	26.9	173.2	0.11
TN-WA	47.9	0.2	148.9	56.7	0.17
TN-A	47.8	0.09	150.1	76.8	0.27

rollup mechanism suggested that TiO_2 was converted into titanate sheets and the resulting titanate sheets subsequently wrapped into the nanotubes (Wei *et al.*, 2005; Ma *et al.*, 2004; Bavykin *et al.*, 2004). Due to the presence of a large number of dangling bonds on the surface of the nanosheets, the warpping process of the nanosheets to form the nanotubes, which reduced the surface-to-volume ratio and eventually lowered the total energy, was thermodynamically favored. Under our preparation conditions, the marked high content of sodium in TN-W indicated that part of titanate existed in sodium form and the titanate was not completely exfoliated to generate the nanosheets. Therefore, nanosheets and particles were obtained in the TEM image of TN-W. After acid exchange, the sodium form of the titanate was converted into protonic form and exfoliated into nanosheets, resulting in the presence of surface unsaturated bonds as well as the increased instability of the nanosheet. This eventually led to the formation of nanotubes in TN-A and TN-WA. For the preparation of TN-A, it is noteworthy that the reaction between HCl with the residual NaOH on TN-P led to a markedly increased salt concentration in the solution. The higher instability of the nanosheets in the solution with higher salt concentration enhanced the rollup of the nanosheets, which accounted for the complete transformation of TiO_2 particles to nanotube in the case of TN-A.

2.2 Adsorption isotherms

In a hetero-catalytic reaction system, the catalytic reaction basically occurs on the surface of the catalyst. Therefore, information about the adsorption of reactants on the surface of the catalyst is very important for understanding the photocatalytic performance of the catalyst.

Adsorption isotherms of Acid-red 3B on the TN-WA and TN-A are presented in Fig.4. The adsorption behaviors of Acid-red 3B on the samples could be well described by the Langmuir adsorption model (Chen *et al.*, 1995):

$$Q_e = Q_0 b C_e / (1 + b C_e) \qquad (2)$$

where Q_e is the equilibrium adsorption amount; Q_0 is the maximum adsorption amount; b is the adsorption constant and C_e is the equilibrium concentration of the dye, respectively.

The maximum adsorption capacities of TN-WA and TN-A for Acid-red 3B adsorption were found to be 8.5 and 18.2 mg/g, respectively. The adsorption of Acid-red 3B onto TN-W was almost undetectable and the markedly low adsorption capacity was exclusively related to its low specific surface area. Considering the similar composition and specific surface area of TN-A to those of TN-WA, the higher pore volume of TN-A sample essentially accounted for its higher adsorption capacity for the dye compared to TN-WA (Table 1). In
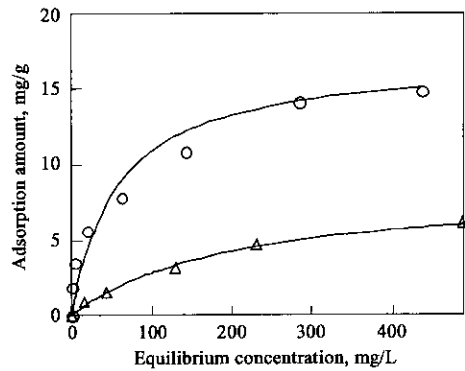

Fig.4 Adsorption isotherms of TN-WA($\triangle$) and TN-A($\bigcirc$)
Solid lines are theoretical fitting curves using Langmuir adsorption model

fact, the enhanced adsorption of the sorbate in the porous materials could be usually achieved due to the strong interaction between the sorbate and the porous sorbent.

2.3 Photocatalytic activity

The time profiles of Acid-red 3B photo-degradation catalyzed by the three different catalysts are compared in Fig.5. Our fitting results showed that the kinetics of Acid-red 3B photo-degradation catalyzed by different catalysts could be well described as pseudo-zero-order kinetics:

$$r = -dC_t / dt = K \qquad (3)$$

$$C_0 - C_t = Kt \qquad (4)$$

where r is the reaction rate; C_t is the concentration of Acid-red 3B at reaction time t, C_0 is the initial concentration of Acid-red 3B and K is the reaction rate constant, respectively.

The reaction rate constant K, reflecting the overall efficiency of the photo-degradation for the Acid-red 3B are listed in Table 2. It is indicated that the presence of the catalyst enhanced the dye degradation and the catalytic efficiency of TN-A is higher than the other two catalysts.
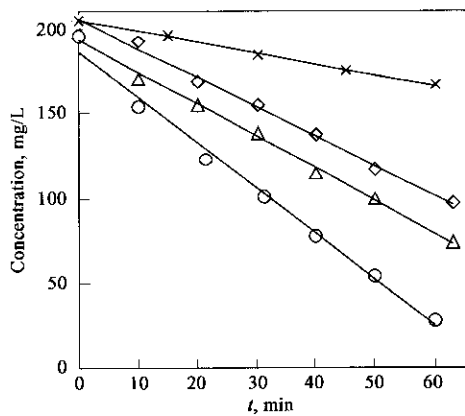

Fig.5 Photo-degradation of Acid-red 3B catalyzed by: ($\Diamond$) TN-W;($\triangle$) TN-WA; ($\bigcirc$)TN-A; ($\times$) blank test. Solid lines are theoretical fitting curves using pseudo-zero-order kinetics model

Table 2 Reaction rate constant K of the three catalysts

Catalyst	K, mg/(L·min)
TN-W	1.7509
TN-WA	1.9151
TN-A	2.6717

In principle, the adsorption properties, the crystalline phases and the crystallinity degree of the photocatalyst were believed to be the most important factors controlling its photocatalytic activity (Masao and Ichiro, 2003). Typically, the photocatalytic removal of aqueous pollutants follows Langmuir-Hinshelwood model (Fox and Dulay, 1993; Zamostny and Belohlav, 2002), indicating the importance of the pre-adsorption of the reactant over the catalyst. In addition, the higher crystallinity degree of the catalyst led to a low surface defects and effectively inhibited the recombination of electron-hole, which led to a higher catalytic efficiency (Sreethawong et al., 2005). Note that the crystallinity degree of the TN-A catalyst was higher than those of TN-W and TN-WA. In addition, the presence of regular nanotubes in TN-A increased the pore volume and simultaneously led to a higher adsorption capacity of TN-A compared to TN-W and TN-WA. Therefore, both the higher crystallinity degree and higher adsorption capacity of TN-A led to a higher photocatalytic activity of TN-A compared to TN-W and TN-WA. This also suggests that the formation of regular nanotubes can enhance the photocatalytic activity of TiO₂ nanotube.

3 Conclusions

TiO₂ nanotubes were prepared using hydro-thermal method followed by different post-treatment, the photo-degradation of Acid-red 3B catalyzed by these catalysts was studied. The results showed that the regular TiO₂ nanotubes could be obtained by direct acid washing. XRD and ICP results showed that TiO₂ nanotube was composed of $H_2Ti_2O_5 \cdot H_2O$. In addition, the increased purity of TiO₂ nanotube effectively enhanced its catalytic activity for Acid-red 3B photo-degradation, which was attributed to its high crystallinity degree and adsorption capacity for Acid-red 3B.

References:

Barbe C J, Arendse F, Comte P et al., 1997. Nanocrystalline titanium oxide electrodes for photovoltaic applications [J]. J Am Ceram Soc, 80: 3157—3171.

Bavykin D B, Parmon V N, Lapkin A A et al., 2004. The effect of hydrothermal conditions on the mesoporous structure of TiO₂ nanotubes[J]. J Mater Chem, 14: 3370—3377.

Chen H Y, Zahraa O, Bouchy M et al., 1995. Adsorption properties of

TiO₂ related to the photocatalytic degradation of organic contaminants in water [J]. J Photochem Photobiol A, 85: 179—186.

Chen Q, Zhou W Z, Du G H et al., 2002. Trititanate nanotubes made via a single alkali treatment[J]. Adv Mater, 14: 1208—1211.

Du G H, Chen Q, Che R C et al., 2001. Preparation and structure analysis of titanium oxide nanotube [J]. Appl Phys Lett, 79: 3702—3704.

Fox M A, Dulay M T, 1993. Heterogeneous photocatalysis [J]. Chem Rev, 93: 341—357.

Ge J T, Qu J H, 2003. Degradation of azo dye acid red B on manganese dioxide in the absence and presence of ultrasonic irradiation[J]. J Hazard Mater, 100: 197—207.

Idakiev V, Yuan Z Y, Tabakova T et al., 2005. Titanium oxide nanotubes as supports of nano-sized gold catalysts for low temperature water-gas shift reaction[J]. Appl Catal A, 281: 149—155.

Kasuga T, Hiramatsu M, Hoson A et al., 1998. Formation of titanium oxide nanotube[J]. Langmuir, 14: 3160—3163.

Kasuga T, Hiramatsu M, Hoson A et al., 1999. Titania nanotubes prepared by chemical processing[J]. Adv Mater, 11: 1307—1311.

Koch M, Yediler A, Lienert D et al., 2002. Ozonation of hydrolyzed azo dye reactive yellow 84 (CI)[J]. Chemosphere, 16: 109—113.

Ma R, Bando Y, Sasaki T, 2003. Nanotubes of lepidocrocite titanates[J]. Chem Phys Lett, 380: 577—582.

Ma R, Bando Y, Sasaki T, 2004. Directly rolling nanosheets into nanotube[J]. J Phys Chem B, 108: 2115—2119.

Masao K, Ichiro O, 2003. Photocatalysis: science and technology[M]. New York: Springer. 29—33.

Saha T K, Karmaker S, Ichikawa H et al., 2005. Mechanisms and kinetics of trisodium 2-hydroxy-1,1′-azonaphthalene-3,4′,6-trisulfonate adsorption onto chitosan [J]. J Colloid Interf Sci, 286: 433—439.

Sreethawong T, Suzuki Y, Yoshikawa S, 2005. Synthesis, characterization, and photocatalytic activity for hydrogen evolution of nanocrystalline mesoporous titania prepared by surfactant-assisted templating sol-gel process [J]. J Solid State Chem, 178: 329—338.

Vinodgopal K, Hotchandani S, Kamat P V, 1993. Electrochemically assisted photocatalysis: titania particulate film electrodes for photocatalytic degradation of 4-chlorophenol [J]. J Phys Chem, 97: 9040—9044.

Wang W Z, Varghese O K, Paulose M et al., 2004. A study on the growth and structure of titania nanotubes[J]. J Mater Res, 19: 417—422.

Wei M D, Konishi Y, Zhou H S et al., 2005. Formation of nanotubes TiO₂ from layered titanate particles by a soft chemical process[J]. Solid State Comm, 133: 493—497.

Yang J J, Jin Z S, Wang X D et al., 2003. Study on composition, structure and formation process of nanotube Na₂Ti₂O₄(OH)₂ [J]. Dalton Trans, 3898—3901.

Yoshida R, Suzuki Y, Yoshikawa S, 2005. Effects of synthetic conditions and heat-treatment on the structure of partially ion-exchanged titanate nanotubes [J]. Mater Chem Phys, 91: 409—416.

Zamostny P, Belohlav Z, 2002. Identification of kinetic models of heterogeneously catalyzed reactions[J]. Appl Catal A, 225: 291—299.

Zhang M, Jin Z S, Zhang J W et al., 2004. Effect of annealing temperature on morphology, structure and photocatalytic behavior of nanotubed H₂Ti₂O₄(OH)₂[J]. J Mol Catal A, 217: 203—210.

Zheng S R, Huang Q G, Zhou J et al., 1997. A study on dye photoremoval in TiO₂ suspension solution [J]. J Photochem Photobiol A, 108: 235—238.

Zheng S R, Zheng J Z, Zou Z G, 2005. Photo-catalytic properties of TiO₂ supported layered compounds for dye removal [J]. Res Chem Intermediat, 31: 493—498.